

## Article

# Ab initio Investigation of Impurity Ferromagnetism in the Pd<sub>1-x</sub>Fe<sub>x</sub> Alloys: Concentration and Position Dependences

Irina Piyanzina <sup>1,2</sup>, Amir Gumarov <sup>1,2,\*</sup>, Rustam Khaibullin <sup>1</sup> and Lenar Tagirov <sup>1,2</sup><sup>1</sup> Zavoisky Physical-Technical Institute, FRC Kazan Scientific Center of RAS, 420029 Kazan, Russia; IIPiyanzina@kpfu.ru (I.P.); rik@kfti.knc.ru (R.K.); Itagirov@mail.ru (L.T.)<sup>2</sup> Institute of Physics, Kazan Federal University, 420008 Kazan, Russia

\* Correspondence: amir@gumarov.ru

**Abstract:** We present the results of *ab initio* studies of the structural and magnetic properties of the Pd host matrix doped by Fe atoms at various concentrations. By means of the density functional theory, we deduce that iron impurities are able to initialize significant magnetization of the Pd atoms, when the impurity concentration exceeds 3 at.%. We also demonstrate that the induced magnetization depends on impurity positions in the host matrix, in particular, there is a maximum of magnetization for a uniform distribution of the iron solute.

**Keywords:** Pd–Fe alloy; impurity ferromagnetism; DFT



**Citation:** Piyanzina, I.; Gumarov, A.; Khaibullin, R.; Tagirov, L. *Ab initio* Investigation of Impurity Ferromagnetism in the Pd<sub>1-x</sub>Fe<sub>x</sub> Alloys: Concentration and Position Dependences. *Crystals* **2021**, *11*, 1257. <https://doi.org/10.3390/cryst11101257>

Academic Editors: Paolo Restuccia and James Ren

Received: 20 September 2021

Accepted: 14 October 2021

Published: 18 October 2021

**Publisher's Note:** MDPI stays neutral with regard to jurisdictional claims in published maps and institutional affiliations.



**Copyright:** © 2021 by the authors. Licensee MDPI, Basel, Switzerland. This article is an open access article distributed under the terms and conditions of the Creative Commons Attribution (CC BY) license (<https://creativecommons.org/licenses/by/4.0/>).

## 1. Introduction

The Pd<sub>1-x</sub>Fe<sub>x</sub> alloys have been known and studied for a long time; pioneering works date back to 1938 by Fallot [1]. Later, in 1960, bulk Pd<sub>1-x</sub>Fe<sub>x</sub> alloys were deeply investigated by Crangle [2]. Experimental findings and their understanding at the time of the 1970s were summarized in a review by Nieuwenhuys [3]. The current revival of interest is fueled by the potential use as a material of a choice for a weak and soft ferromagnet in superconducting Josephson magnetic random-access memory (MRAM) based on Josephson junctions [4–13]. The Pd-rich ferromagnetic Pd<sub>1-x</sub>Fe<sub>x</sub> ( $0.01 < x < 0.1$ ) alloy is used there in the form of a thin film fabricated utilizing magnetron sputtering [5–11,13–15], molecular-beam epitaxy (MBE) [15–23], and ion-beam implantation [24].

There is a scatter of opinions on the compositional and magnetic homogeneity of Pd<sub>1-x</sub>Fe<sub>x</sub> films obtained by different deposition techniques: some papers report an indication of clustering [10,11,13,14] or formation of the nanograins of the Pd<sub>3</sub>Fe phase [15] in samples deposited with the magnetron sputtering technique; the others on MBE growth of thin Pd<sub>1-x</sub>Fe<sub>x</sub> films [18–23] report on their high magnetic homogeneity; finally, the ion-implanted palladium films [24] show a significant influence of the Fe implant distribution on saturation magnetization ( $M_s$ ) and Curie temperature ( $T_C$ ) of the samples. It is not clear why and how the redistribution of iron solute in the Pd matrix influences  $M_s$  and  $T_C$ .

From very few existing studies of the electronic structure of Pd<sub>1-x</sub>Fe<sub>x</sub> solid solutions, the Korringa–Kohn–Rostoker Green's function method with the local density functional approximation was used to calculate the magnetic moment at the palladium site in the dilute substitutions ( $x$  close to 1.0) of Pd in bcc Fe [25], while the electronic structures and magnetic properties of Pd<sub>1-x</sub>Fe<sub>x</sub> alloys with  $0.5 \leq x \leq 0.85$  were investigated in the framework of density functional theory (DFT), using the full potential approximation [26]. The only study in a Pd-rich side is [27], where the magnetic properties of palladium–iron alloys and compounds were calculated by means of the spin-polarized and scalar relativistic tight-binding linear muffin tin orbital method (TB-LMTO) within atomic sphere approximation (ASA), together with the coherent potential approximation (CPA) to describe random Pd–Fe solutions. Another very recent study should be mentioned, where DFT calculations of the formation energy of the possible phases in Fe–Pd binary alloys were

investigated [28]. However, magnetic moments and Curie temperatures at  $x < 0.1$  were not presented; therefore, the calculations of [27,28] are not applicable to Pd-rich alloys.

In this work, we perform *ab initio* calculations for the  $\text{Pd}_{1-x}\text{Fe}_x$  alloy with the iron dopant uniformly distributed over the bulk Pd host lattice at the different iron content  $x < 0.1$  and calculate the mean magnetic moment per Fe solute atom and the maximal magnetic moment located on a Pd atom as a function of  $x$ . Then, we study the influence of inhomogeneity in the iron dopant distribution on the magnetic moment per Fe atom and the size and shape of the magnetized “bubble” of the host Pd atoms around the Fe aggregates.

## 2. Computational Details

Our *ab initio* investigations were based on the DFT [29,30] approach within the VASP code [31–33] as a part of the MedeA® software of Materials Design [34]. Exchange and correlation effects were accounted for by the generalized gradient approximation (GGA) as parameterized by Perdew, Burke, and Ernzerhof (PBE) [35]. The Kohn–Sham equations were solved, using the plane-wave basis set (PAW) [36]. The cut-off energy was chosen to be equal to 400 eV. The force tolerance was 0.5 eV/nm and the energy tolerance for the self-consistency loop was  $10^{-5}$  eV. The Brillouin zones were sampled using Monkhorst–Pack grids [37], including  $3 \times 3 \times 3$  k-points. We performed spin-polarized calculations in all cases, initializing Fe atoms to have  $3.63 \mu_B$ , and Pd atoms to be in the paramagnetic state ( $0 \mu_B$ ). The structures are described as consisting of a filled FCC host matrix formed by Pd atoms, with Fe ions substituting octahedrally coordinated sites only (see Figure 1). For the  $3 \times 3 \times 3$  unit cell parameter,  $a = 11.8 \text{\AA}$ .

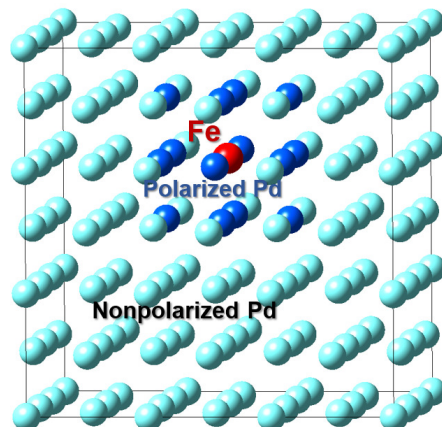


**Figure 1.** Supercell of  $\text{Pd}_{0.98}\text{Fe}_{0.02}$  matrix used in our calculations with denoted polarized Pd atoms around the Fe solute ion after the optimization procedure. Red sphere of atom corresponds to Fe, light blue to Pd, and blue to predominantly polarized Pd atoms.

## 3. Results

### 3.1. Magnetic Properties of $\text{Pd}_{1-x}\text{Fe}_x$ with Varying Concentration and Uniform Impurity Distribution

At the first stage, various concentrations of Fe solute in a  $3 \times 3 \times 3$  Pd-supercell with uniform distribution were considered. We increased the number of Fe atoms in the unit supercell from 1 to 11 by substituting Pd ions. At low  $\text{Fe}^+$  contents ( $x = 0.01$  to 0.03), we obtained a negligible cell magnetization (Figure 2a). At such concentrations, Fe solute atoms are non-magnetic (Figure 2b) and do not magnetize the surrounding Pd atoms. As the impurity concentration increases, iron becomes magnetic (Figure 2b) and magnetizes the surrounding Pd atoms (Figure 3a). In particular, about 14 Pd atoms received significant magnetic moments, as shown in Figure 1. We found that the total magnetization of a cell with seven Fe solute atoms gives rise to the highest total magnetic moment calculated per Fe atom, which equals  $\approx 8 \mu_B$  (including Fe magnetic moment). This value is in agreement with the experimental results shown also in Figure 2a. After the

peak point, the curve slowly decreases, in agreement with the results of Esmaeili et al. [21] obtained for MBE films, and of Crangle [2] found for the bulk. Our curve is somewhere in the middle of two mentioned results. However, there is a contradiction with experiment at low impurity concentrations. That might be due to the fact that the calculations were performed assuming 0 K, and we obtained Fe solute atoms, as a result of optimization, as being non-magnetic at low impurity concentrations, whereas experimental measurements were carried out at final temperatures. The theory of impurity ferromagnetism suggests that at a very low impurity concentration, when the distance between the impurity ions is large enough, the oscillatory potential prevails over the ferromagnetic one so that the impurity ferromagnetism does not occur, and the spin glass is formed in the alloy [38]. In comparison with the assumed theoretical value of  $x = 10^{-4}$  [38] for the critical Fe content, *ab initio* gives  $x = 0.03$ .

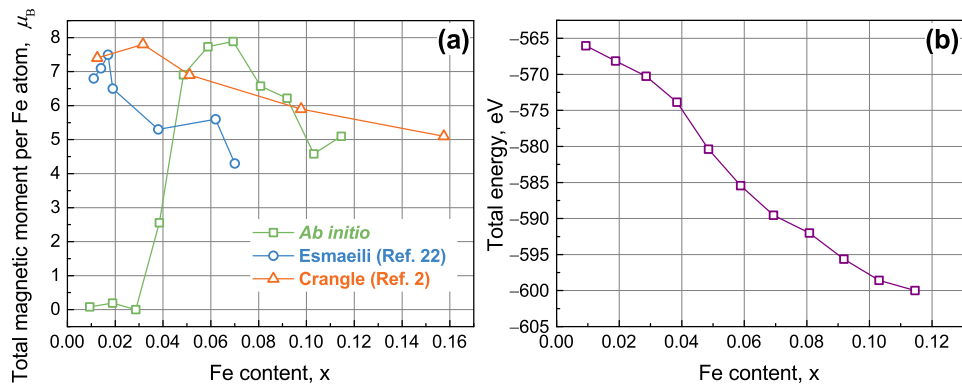


**Figure 2.** (a) Total magnetic moment calculated per Fe solute atom versus Fe content in the  $3 \times 3 \times 3$  Pd supercell (green line with squares), along with the experimental data plotted for MBE film (blue line with circles) and for the bulk (red line with triangles) taken from references [2,21], respectively; (b) Energy decrease with increase in the Fe atoms content  $x$ . Here, the total energy was calculated per  $3 \times 3 \times 3$  Pd supercell with uniform distribution of the Fe solute atoms.

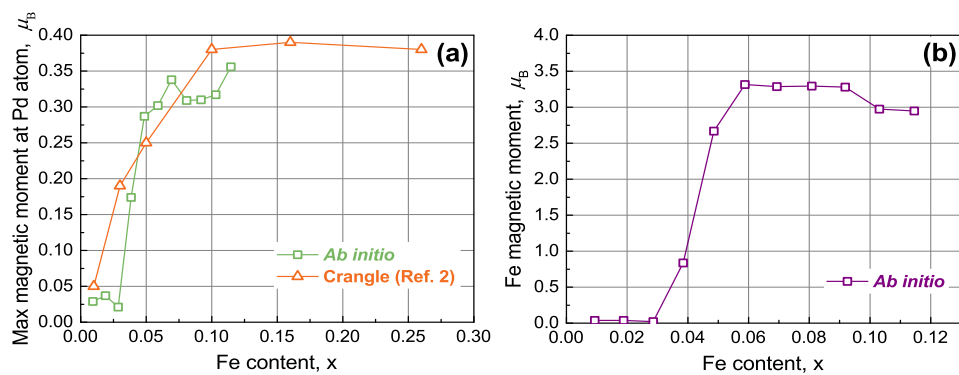


**Figure 3.** (a) Maximal magnetic moment calculated for a Pd atom versus the  $\text{Fe}^+$  atoms content in a  $3 \times 3 \times 3$  Pd supercell with uniform impurity distribution (green line with squares) along with the experimental data for the bulk alloy [2] (red line with triangles); (b) The calculated average magnetic moment per Fe atom with the uniform impurity distribution.

At the same time, the calculated magnetic moments for Pd atoms are in a very good agreement with the experimental data obtained by Crangle [2] for bulk alloys (Figure 3a). One can notice that the magnetic moment of Pd sharply increases from  $\approx 0.05$  to  $0.35 \mu_B$  when the iron concentration exceeds three atoms per  $3 \times 3 \times 3$  cell. After that, the magnetic moment reaches a plateau with the highest value of the moment per Pd atom being equal to  $\approx 0.35 \mu_B$ , which is consistent with the experimental data shown also in Figure 3a. The magnetic moment of iron also reaches a plateau with a constant value of  $\approx 3.25 \mu_B$ .

(Figure 3b), which is lower than the theoretical maximum, but it is higher than the value of  $2.8 \mu_B$  obtained in [2] and close to the value of  $3.5 \mu_B$  obtained by Neutron diffraction experiments [39,40]. We also checked the concentration dependence of the total energy, which shows a descending character and might mean that the system tends to have Fe ions in the matrix (Figure 2b).

The discussed findings confirm the reproducibility of the experimental results [2,21] as well as the theoretical predictions [38] for  $Pd_{1-x}Fe_x$  alloys with the *ab initio* instrument, which will be used in further discussions regarding the positions of Fe impurities in the host matrix.

### 3.2. $Pd_{0.98}Fe_{0.02}$ : Impurity Position Impact

At the second stage, we consider the influence of Fe–Fe distance in the alloy with  $Pd_{0.98}Fe_{0.02}$  composition if two iron solute atoms reside in the  $3 \times 3 \times 3$  Pd supercell. We found that at particular distances ( $\approx 6 \text{ \AA}$ ), the total magnetization as well as the magnetic moment per Pd atom reach a wide maximum (Figure 4a). The highest total magnetization per Fe atom equals  $\approx 7.6 \mu_B$ , while the highest magnetic moment of the Pd atom is  $\approx 0.2 \mu_B$  (Figure 4c). This maximum of magnetization corresponds to the minimum of the total energy (Figure 4b). We also tested a different (another concentration) configuration of three Fe solute atoms in the host Pd supercell and obtained similar dependence with a maximum of magnetization at analogous Fe–Fe distances.

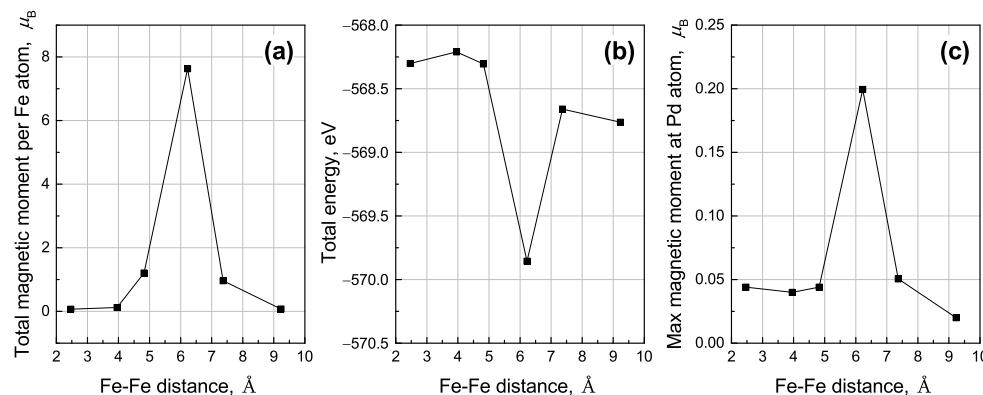


**Figure 4.** (a) Total magnetic moment calculated per  $Fe^+$  ion plotted against Fe to Fe distance; (b) total energy of the  $3 \times 3 \times 3$  Pd supercell; (c) maximal magnetic moment at Pd atom. Two substitutional Fe atoms in the host matrix cell were considered. Each point was obtained by averaging over at least three configurations when Fe atom substitutes for Pd in different lattice sites but at the same interatomic distance.

With this finding, we may claim that magnetization depends on the impurity distribution. The maximum of the total magnetization could be achieved at a particular distance between Fe solute atoms. With this arrangement of the iron impurity, the maximum number of polarized palladium atoms participate in the long-range magnetic order (thereby creating an infinite cluster), which leads to a noticeable change in the magnetic properties—an increase in the magnetization and Curie temperature. Indeed, in [24], it was demonstrated that the annealing process changed the total magnetization as well as the Curie temperature of the Pd samples. After implantation for the samples preparation, Fe-impurities are distributed inhomogeneously in the Pd matrix. However, further thermal annealing leads to a more uniform redistribution of impurities in the host Pd matrix, and, consequently, to the increase in the number of polarized palladium clouds participating in the long-range magnetic order. As can be seen from Figure 4b, this magnetization increase corresponds to the system with lower energy. Obviously, the system tends to have the lowest energy, and this may happen during the annealing process. This is illustrated in Figure 5, where three possible iron configurations are discussed.

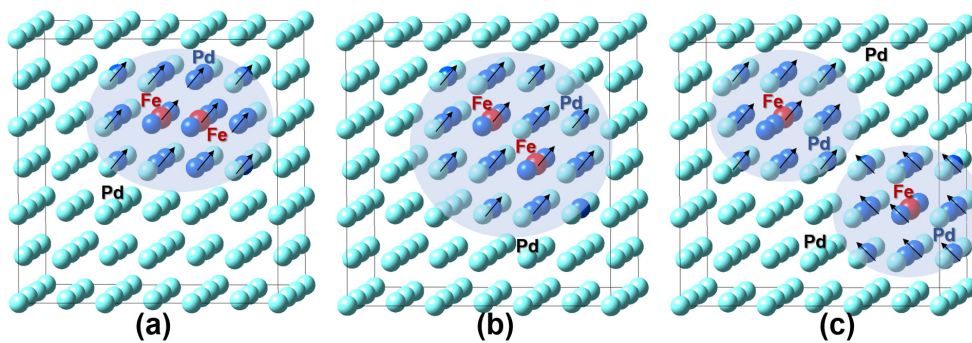


**Figure 5.** Magnetic clusters formed around Fe solute atom impurities in the  $3 \times 3 \times 3$  Pd host matrix. Three configurations are shown: (a) Fe atoms are located close to each other; (b) further away; (c) at a distance. Red spheres of atoms correspond to Fe, light blue to Pd, and blue to predominantly polarized Pd atoms. Transparent blue spheres outline magnetic clusters formed around magnetic impurities, and black arrows denote one special case of magnetic moments orientation.

Closely located magnetic impurities (Figure 5a) form two overlapping magnetic clusters of neighboring Pd atoms. This situation is energetically unfavorable and the system of  $\text{Pd}_{0.98}\text{Fe}_{0.02}$  has a relatively low total magnetic moment  $\approx 0.5 \mu_B$  (Figure 4a) calculated per Fe atom. As soon as the solute atoms move away from each other (during annealing, for instance) (Figure 5b), the total energy lowers reaching a minimum (Figure 4c). This energy minimum corresponds to the maximum of magnetization ( $\approx 7.6 \mu_B$  at  $6\text{\AA}$  in Figure 4a) and the solute atoms configuration depicted in Figure 5b. Finally, distant magnetic clusters (Figure 5c) weakly feel each other and may even have opposite magnetic moment directions, which results in low spontaneous magnetization and higher energy.

#### 4. Conclusions

In the present work, we have demonstrated that calculations within the density functional theory can reproduce basic experimental results obtained for  $\text{Pd}_{1-x}\text{Fe}_x$  alloys. In particular, we have shown that the Fe solute in Pd host matrix induces ferromagnetism, which extends to very low concentrations ( $x = 0.03$ ). The magnitude of the total magnetic moment is very large, about  $7.6 \mu_B$  per Fe solute atom, and it smoothly decreases with increasing the impurity concentration.

We also investigated the dependence of magnetization on the mutual positions of dissolved Fe in the Pd host matrix. The aim was to answer the experimental question about the nature of the increase in  $T_C$  and  $M$  upon annealing. We have demonstrated that the magnitude of the total magnetic moment of  $\text{Pd}_{0.98}\text{Fe}_{0.02}$  alloy depends on the impurity positions; as a consequence, the magnetization increase during annealing relates to the impurity redistribution in the Pd matrix.

**Author Contributions:** Conceptualization, A.G. and I.P.; methodology, I.P.; software, I.P.; validation, A.G. and L.T.; formal analysis, I.P.; investigation, I.P.; resources, I.P.; data curation, I.P. and A.G.; writing—original draft preparation, I.P.; writing—review and editing, A.G. and L.T.; visualization, A.G.; supervision, L.T.; project administration, R.K.; funding acquisition, R.K. All authors have read and agreed to the published version of the manuscript.

**Funding:** This work was supported by RFBR Grant No. 20-02-00981.

**Institutional Review Board Statement:** Not applicable.

**Informed Consent Statement:** Not applicable.

**Data Availability Statement:** Not applicable.

**Acknowledgments:** Computing resources were provided by Laboratory of Computer design of new materials in Kazan Federal University. The authors thank Igor Yanilkin and Roman Yusupov from Kazan Federal University for stimulating discussions.

**Conflicts of Interest:** The authors declare no conflict of interest.

## References

1. Fallot, M. Les alliages du fer avec les métaux de la famille du platine. *Ann. Phys.* **1938**, *11*, 291–332. [[CrossRef](#)]
2. Crangle, J. Ferromagnetism in Pd-rich palladium-iron alloys. *Philos. Mag.* **1960**, *5*, 335–342. [[CrossRef](#)]
3. Nieuwenhuys, G.J. Magnetic behaviour of cobalt, iron and manganese dissolved in palladium. *Adv. Phys.* **1975**, *24*, 515–591. [[CrossRef](#)]
4. Ryazanov, V.V. Josephson superconductor—ferromagnet—superconductor  $\pi$ -contact as an element of a quantum bit (experiment). *Uspekhi Fiz. Nauk* **1999**, *42*, 825–827. [[CrossRef](#)]
5. Arham, H.Z.; Khaire T.S.; Loloei, R.; Pratt W.P.; Birge, N.O. Measurement of spin memory lengths in PdNi and PdFe ferromagnetic alloys. *Phys. Rev. B* **2009**, *80*, 52–62. [[CrossRef](#)]
6. Bol'ginov, V.V.; Tikhomirov, O.A.; Uspenskaya, L.S.; Two-Component Magnetization in Pd<sub>99</sub>Fe<sub>01</sub> Thin Films. *JETP Lett.* **2017**, *105*, 169–173. [[CrossRef](#)]
7. Larkin, T.I.; Bol'ginov, V.V.; Stolyarov, V.S.; Ryazanov, V.V.; Vernik, I.V.; Tolpygo, S.K.; Mukhanov, O.A. Ferromagnetic Josephson switching device with high characteristic voltage. *Appl. Phys. Lett.* **2012**, *100*, 222601. [[CrossRef](#)]
8. Ryazanov, V.V.; Bol'ginov, V.V.; Sobanin, D.S.; Vernik, I.V.; Tolpygo, S.K.; Kadin, A.M.; Mukhanov, O.A. Magnetic Josephson junction technology for digital and memory applications. *Phys. Procedia* **2012**, *36*, 35–41. [[CrossRef](#)]
9. Vernik, I. V.; Bol'ginov, V.V.; Bakurskiy, S.V.; Golubov, A.A.; Kupriyanov, M.Y.; Ryazanov, V.V.; Mukhanov, O.A. Magnetic Josephson junctions with superconducting interlayer for cryogenic memory. *IEEE Trans. Appl. Supercond.* **2013**, *23*, 1701208. [[CrossRef](#)]
10. Niedzielski, B.M.; Diesch, S. G.; Gingrich, E.C.; Wang, Y.; Loloei, R.; Pratt, W.P.; Birge, N. O. Use of Pd–Fe and Ni–Fe–Nb as Soft Magnetic Layers in Ferromagnetic Josephson Junctions for Nonvolatile Cryogenic Memory. *IEEE Trans. Appl. Supercond.* **2014**, *24*, 1800307. [[CrossRef](#)]
11. Glick, J.A.; Loloei, R.; Pratt, W.P.; Birge, N.O. Critical current oscillations of Josephson junctions containing PdFe nanomagnets. *IEEE Trans. Appl. Supercond.* **2016**, *27*, 1800205. [[CrossRef](#)]
12. Soloviev, I.I.; Klenov, N.V.; Bakurskiy, S. V.; Kupriyanov, M.Y.; Gudkov, A.L.; Sidorenko, A.S. Beyond Moore's technologies: operation principles of a superconductor alternative. *Beilstein J. Nanotechnol.* **2017**, *8*, 2689–2710. [[CrossRef](#)]
13. Uspenskaya, L.S.; Rakhmanov, A.L.; Dorosinskii, L.A.; Chugunov, A.A.; Stolyarov, V.S.; Skryabina, O.V.; Egorov, S.V. Magnetic Patterns and Flux Pinning in Pd<sub>0.99</sub>Fe<sub>0.01</sub>–Nb Hybrid Structures. *JETP Letters* **2013**, *97*, 155–158. [[CrossRef](#)]
14. Uspenskaya, L.S.; Rakhmanov, A.L.; Dorosinskii, L.A.; Bozhko, S.I.; Stolyarov, V.S.; Bol'ginov, V.V. Magnetism of ultrathin Pd<sub>99</sub>Fe<sub>01</sub> films grown on niobium. *Mater. Res. Express* **2014**, *1*, 036104. [[CrossRef](#)]
15. Uspenskaya, L.S.; Shashkov, I.V. Influence of Pd<sub>0.99</sub>Fe<sub>0.01</sub> film thickness on magnetic properties. *Phys. B Condens. Matter* **2018**, *549*, 58–61. [[CrossRef](#)]
16. Garifullin, I.A.; Tikhonov, D.A.; Garif'yanov, N.N.; Fattakhov, M.Z.; Theis-Bröhl, K.; Westerholt, K.; Zabel, H. Possible Reconstruction of the Ferromagnetic State under the Influence of Superconductivity in Epitaxial V/Pd<sub>1-x</sub>Fe<sub>x</sub> Bilayers. *Appl. Magn. Reson.* **2002**, *22*, 439–452. [[CrossRef](#)]
17. Ewerlin, M.; Pfau, B.; Günther, C. M.; Schaffert, S.; Eisebitt, S.; Abrudan, R.; Zabel, H. Exploration of magnetic fluctuations in PdFe films. *J. Phys. Condens. Matter* **2013**, *25*, 266001. [[CrossRef](#)]
18. Esmaeili, A.; Vakhitov, I.R.; Yanilkin, I.V.; Gumarov, A.I.; Khaliulin, B.M.; Gabbasov, B.F.; Aliyev, M.N.; Yusupov, R.V.; Tagirov, L.R. FMR Studies of Ultra-Thin Epitaxial Pd<sub>0.92</sub>Fe<sub>0.08</sub> Film. *Appl. Magn. Reson.* **2018**, *49*, 175–183. [[CrossRef](#)]
19. Esmaeili, A.; Yanilkin, I.V.; Gumarov, A.I.; Vakhitov, I.R.; Gabbasov, B.F.; Kiiamov, A.G.; Rogov, A.M.; Osin, Y.N.; Denisov, A.E.; Yusupov, R.V.; Tagirov, L.R. Epitaxial growth of Pd<sub>1-x</sub>Fe<sub>x</sub> films on MgO single-crystal substrate. *Thin Solid Films* **2019**, *669*, 338–344. [[CrossRef](#)]
20. Petrov, A.V.; Yusupov, R.V.; Nikitin, S.I.; Gumarov, A.I.; Yanilkin, I.V.; Kiiamov, A.G.; Tagirov, L.R. Femtosecond optical and magneto-optical spectroscopy study of magnetic and electronic inhomogeneities in a Pd<sub>0.94</sub>Fe<sub>0.06</sub> thin film. *JETP Lett.* **2019**, *109*, 266–269. [[CrossRef](#)]
21. Esmaeili, A.; Yanilkin, I.V.; Gumarov, A.I.; Vakhitov, I.R.; Yusupov, R.V.; Tatarsky, D.A.; Tagirov, L.R. Epitaxial thin-film Pd<sub>1-x</sub>Fe<sub>x</sub> alloy—A tunable ferromagnet for superconducting spintronics. *Sci. China Mater.* **2021**, *64*, 1246–1255. [[CrossRef](#)]
22. Mohammed, W.M.; Yanilkin, I.V.; Gumarov, A.I.; Kiiamov, A.G.; Yusupov, R.V.; Tagirov, L.R. Epitaxial growth and superconducting properties of thin-film PdFe/VN and VN/PdFe bilayers on MgO(001) substrates. *Beilstein J. Nanotechnol.* **2020**, *11*, 807–813. [[CrossRef](#)]
23. Yanilkin, I.V.; Mohammed, W.M.; Gumarov, A.I.; Kiiamov, A.G.; Yusupov, R.V.; Tagirov, L.R. Synthesis, characterization, and magnetoresistive properties of the epitaxial Pd<sub>0.96</sub>Fe<sub>0.04</sub>/VN/Pd<sub>0.92</sub>Fe<sub>0.08</sub> superconducting spin-valve heterostructure. *Nanomaterials* **2021**, *11*, 64. [[CrossRef](#)] [[PubMed](#)]
24. Gumarov, A.I.; Yanilkin, I.V.; Yusupov, R.V.; Kiiamov, A.G.; Tagirov, L.R.; Khaibullin, R.I. Iron-implanted epitaxial palladium thin films: Structure, ferromagnetism and signatures of spinodal decomposition. *Mater. Lett.* **2021**, *305*, 130783. [[CrossRef](#)]
25. Opahle, I.; Koepernik, K.; Nitzsche, U.; Richter, M. Effect of external pressure on the Fe magnetic moment in undoped LaFeAsO from density functional theory: Proximity to a magnetic instability. *Appl. Phys. Lett.* **2009**, *94*, 072508. [[CrossRef](#)]
26. Drittler, B.; Stefanou, N.; Blügel, S.; Zeller, R.; Dederichs, P.H. Electronic structure and magnetic properties of dilute Fe alloys with transition-metal impurities. *Phys. Rev. B* **1989**, *40*, 8203–8212. [[CrossRef](#)]

27. Burzo, E.; Vlaic, P. Magnetic and magnetocaloric properties of some ferrimagnetic compounds. *J. Optoelectron. Adv. Mater.* **2010**, *12*, 1105–1113.
28. Pathaka, R.; Golovnia, O.A.; Gerasimov, E.G.; Popov, A.G.; Vlasov, N.I.; Skomski, R.; Kashyap, A. Ab initio study of the magnetic properties of possible phases in binary Fe-Pd alloys. *J. Magn. Magn. Mater.* **2020**, *499*, 166266. [[CrossRef](#)]
29. Hohenberg, P.; Kohn, W. Inhomogeneous Electron Gas. *Phys. Rev.* **1964**, *136*, B864–B871. [[CrossRef](#)]
30. Kohn, W.; Sham, L.J.; Self-Consistent Equations Including Exchange and Correlation Effects. *Phys. Rev.* **1965**, *140*, A1133–A1138. [[CrossRef](#)]
31. Kresse, G.; Furthmüller, J. Efficiency of ab-initio total energy calculations for metals and semiconductors using a plane-wave basis set. *Comp. Mat. Sci.* **1996**, *6*, 15–50. [[CrossRef](#)]
32. Kresse, G.; Furthmüller, J. Efficient iterative schemes for ab initio total-energy calculations using a plane-wave basis set. *Phys. Rev. B* **1996**, *54*, 11169–11186. [[CrossRef](#)]
33. Kresse, G.; Joubert, D. From ultrasoft pseudopotentials to the projector augmented-wave method. *Phys. Rev. B* **1999**, *59*, 1758–1775. [[CrossRef](#)]
34. MedeA Version 2.20; MedeA Software: San Diego, CA, USA, 2018.
35. Perdew, J.P.; Burke K.; Ernzerhof, M. Generalized Gradient Approximation Made Simple. *Phys. Rev. Lett.* **1996**, *77*, 3865–3868. [[CrossRef](#)] [[PubMed](#)]
36. Blöchl, P.E. Projector augmented-wave method. *Phys. Rev. B* **1994**, *50*, 17953–17979. [[CrossRef](#)] [[PubMed](#)]
37. Monkhorst, H.J.; Pack, J.D. Special points for Brillouin-zone integrations. *Phys. Rev. B* **1976**, *13*, 5188–5192. [[CrossRef](#)]
38. Korenblit, I.Y.; Shender, E.F. Ferromagnetism of disordered systems. *Sov. Phys. Uspekhi* **1978**, *21*, 832–851. [[CrossRef](#)]
39. Low, G.G. The electronic structure of some transition metal alloys. *Adv. Phys.* **1969**, *18*, 371–400. [[CrossRef](#)]
40. Aldred, A.T.; Rainford, B.D.; Stringfellow, M.W. Magnetic Moment Distribution in Dilute Alloys of Nickel in Palladium. *Phys. Rev. Lett.* **1970**, *24*, 897–900. [[CrossRef](#)]